IJCRT.ORG ISSN : 2320-2882

INTERNATIONAL JOURNAL OF CREATIVE RESEARCH THOUGHTS (IJCRT)

An International Open Access, Peer-reviewed, Refereed Journal

# Docking, vibrational and optic properties of 2,3,5-trichlorobenzophenol spectroscopic studies as well as DFT quantum chemical calculations

M. Govindarajan[a, b*],

[a]*Department of Physics, Avvaiyar Government College for Women (AGCW),Karaikal , Puducherry 609 602, India*

[b] *Arignar Anna Government Arts and Science College for Women (AAGASC),Karaikal Puducherry 609602, India*

**Abstract**

The conformational analysis was used through the potential surface scan in order to determine the most optimized geometry of the 2,3,5-trichlorobenzophenol molecule (235TCBP). Experimental FT-IR and FT-Raman and NMR spectra were recorded. Hirshfeld surface analysis is found for the compound. The molecular geometry and vibrational wavenumbers in the were calculated by using the Hartree-Fock (HF) and density functional theory (DFT) methods (B3LYP) with 6-311++G(d,p) basis set. Comparison of the observed wavenumbers of 235TCBP with calculated results by HF and DFT indicates that B3LYP is excellent. The differences between the observed and calculated wavenumber values are very small. The theoretically calculated FT-IR and FT-Raman spectra of the title molecule have been constructed. A study on the electronic properties, such as HOMO, HOMO-1, LUMO and LUMO+1 energy was performed by this molecule. Molecular electrostatic potential (MSP) and thermodynamic properties were performed. The molecular docking activity is available in target chlorine and the oxygen atom analyzing the molecular mechanisms of ligand recognition. Atomic charges of 235TCBP was calculated and compared with molecule.

**Keywords:** Vibrational spectra; 2,3,5-trichlorobenzophenol; HF and DFT calculations; HOMO-LUMO.

## 1. Introduction

Catalytic dichlorination of 235TCBP is used to prepare palladium film-modified titanium mesh conductor. The factor determines, such as Pd2+ concentration, plating solution pH, and electrodeposition time and current, on the formulation of the electrode were studied by cyclic voltammetry to establish the optimal electrode preparation conditions [1]. Catalytic hydrochlorination of 235TCBP was analyzed over 0.97%Pd/C, 0.98%Rh/C, and 0.8%Pd/0.19%Rh/C catalysts in various methanol/water mixtures. This is also 2,3,5-trichlorophenol was sped up by changing the part of methanol in water/methanol mixtures up to 50% (v/v), and beyond, where the reaction rate was slowed down [2]. The intermediates of degradation were 2,4,6-trichlorophenol, 2,4-dichlorophenol, 4-chlorophenol, 235TCBP, 3,5-dichlorophenol, and 3-chlorophenol; lower concentrations of these intermediates were observed in the presence of zinc [3]. An actinomycete, Rhodococcus chlorophenolicus, isolated from a pentachlorophenol-degrading mixed bacterial culture is a polychlorophenol degrader. It was established to oxidize pentachlorophenol into carbon dioxide and to metabolize also 2,3,4,5-,2,3,4,6-, and 2,3,5,6-tetrachlorophenol, 2,3,4-, 2,3,5-, 2,3,6-, 2,4,6-, and 2,4,5-trichlorophenol, 2,5-, and 2,6-dichlorophenol and tetrachloro-p-hydroquinone in an inducible manner. Other chlorophenols mentioned were able to set on the synthesis of enzymes for their own degradation. 2,3,4,5-, and 2,3,4,6-tetrachlorophenol, and 2,3,5-, 2,4,5-, and 3,4,5-trichlorophenol were more toxic to R [4].

The photocatalytic degradation of four chlorinated aromatic compounds, namely pentachlorophenol, 2,4-dichlorophenol, 3,5-dichlorophenol, and 235TCBP was looked into the presence of an aqueous of TiO2 irradiated with near-UV light. Only in the case of pentachlorophenol and 235TCBP were the intermediates, identified by HPLC and GC/MS, found to be more toxic than the parent compound.

This bacterium dechlorinates various different chlorophenols at ortho, meta, and para positions; exceptions to this are 2,3-dichlorophenol, 2,5-dichlorophenol, 3,4-dichlorophenol, and the monochlorophenols. The time course of pentachlorophenol dechlorination suggests that two enzyme systems are involved in dehalogenation in strain PCP-1T [5].

## 2. Experimental details

The compound under investigation namely 235TCBP is purchased from M/S Aldrich Chemicals, (USA) with spectroscopic grade and it is used as such without any further purification. The FT-IR spectrum of the compound was recorded in Perkin-Elmer 180 Spectrometer between 4000–100 $cm^{-1}$. The spectral resolution is ± 2 $cm^{-1}$. The FT-Raman spectrum of the compound was also recorded in the same instrument with FRA 106 Raman module equipped with Nd: YAG laser source operating at 1.064 μm line widths with 200 mW powers. The spectra were recorded with scanning speed of 30 $cm^{-1}$ $min^{-1}$ of spectral width 2 $cm^{-1}$. The frequencies of all sharp bands are accurate to ± 1 $cm^{-1}$.

## 3. Quantum chemical calculations

The quantum chemical calculations have been fitted at HF and DFT (B3LYP) methods with 6-311++G(d,p) basis sets using the Gaussian 09W program [7]. The optimized molecule parameters have been evaluated for the calculations of vibrational frequencies by assuming Cs point group symmetry. At the optimized geometry for the title molecule no imaginary frequency modes were obtained, therefore there is a true minimum on the potential energy surface was found. As a result, the unscaled calculated frequencies, infrared intensities, Raman activities and depolarization ratios are obtained. In order to fit the theoretical wavenumbers to the experimental, the scaling factors have been introduced by using a least square optimization of the computed to the experimental data. Vibrational frequencies are scaled as 0.9067 for HF and the range of wavenumbers above 1700 $cm^{-1}$ are scaled as 0.958 and below 1700 $cm^{-1}$ scaled as 0.983 for B3LYP [8] to account for systematic errors caused by basis set incompleteness, neglect of electron correlation and vibrational anharmonicity. After scaled with the scaling factor, the deviation from the experiments is less than 10 $cm^{-1}$ with a few exceptions. The assignments of the calculated normal modes have been made on the basis of the corresponding PEDs. The PEDs are computed from quantum chemically calculated vibrational frequencies using VEDA program [9]. Gauss view program [10] has been considered to get visual animation and for the verification of the normal modes assignment.

The electronic absorption spectra for optimized molecule calculated with the time dependent DFT (TD-DFT) at B3LYP/6-311++G(d,p) level in gas phase and solvent (acetone, DMSO and chloroform). The changes in the thermodynamic functions (the heat capacity, entropy, and enthalpy) were investigated for the different temperatures from the vibrational frequency calculations of title molecule. NMR of the molecule is verified with the experimental data and it is maximum coincides with theoretical one. The crystal explorer is also provided with the necessary diagrams. The molecular modelling is produced a docking of the molecule. The MSP and ESP diagrams is indicated the charges oriented with the molecule.

## 4. Results and discussion

### 4.1. Potential energy scan

A potential energy scan is mainly used to describe the relationship between potential energy and molecular geometry. The conformational molecule diagram was used through the potential surface scan in order to determine the most optimized geometry of the 235TCBP molecule. The first potential energy scan 1 curve is carried out with dihedral angle C5-C6-O12-H13 the link between the benzene ring and OH group, respectively. During the scan, all the geometrical parameters were simultaneously relaxed and were varied in steps of 30˚ from 0 to 360˚. and the second potential energy scan 2 curve is carried with dihedral angle C1-C6-O12-H13 the link between the same two groups. The two curves of the potential energy as a function of the dihedral angle were presented in Fig 1 and the values are tabulated in the Table 1. In mixing the two curves, the optimized geometry of molecule is not obtained and the molecule is in a collapsed manner. In this, the minimum energy potential energy would be equal to -0.0708054 hartree. One conformer is obtained out of 11 conformers. The energies of the conformers of the 235TCBP molecule were calculated by AM1

theory. But in structure optimization of the 235TCBP molecule with same diagram in Fig .2 and energy is calculated by B3LYP/6-311++G (d,p) basis method is approximately -1686.415 a.u.

**4.2. Optimized molecular structure**

235TCBP is substituted with two different functional groups and they are hydroxyl bond (OH) and chlorine group in a three positions of a benzene ring. The optimized geometry of 235TCBP which performed by HF and B3LYP methods with atoms numbering is shown in Fig. 2. The optimized bond lengths and bond angles of title compound are given in Table 2. From Table 2, it is found that the dihedral angles no significant variation by DFT/B3LYP and HF methods. So, omit the reading in tabulation. The ring appears little distorted and the angles slightly out of perfect hexagonal structure. In this work, molecular optimization parameters for 235TCBP have been employed without symmetry constrain. The bond lengths HF are slightly better than the B3LYP geometry. The arrangement for bond angles is not as good as that for the bond distances.

The average bond distances of C-C and C-H in the benzene ring calculated by B3LYP and HF method are 1.3941 and 1.3833 and 1.0830 and 1.0735 Å, respectively. The experimental bond lengths of C1–C2 and C1–C6 are more than the theoretical bond lengths. But, the three bond lengths C2-C3, C3-C4, C4-C5 and C5-C6 are B3LYP is slightly more than the experimental bond lengths [6]. The optimized OH (hydroxyl group) bond length are calculated 0.963 and 0941 Å by B3LYP and HF. The C-O bond length is shorter in experimental in comparison with B3LYP than HF values.

The O-H bond length indicates a considerable decrease when substituted in place of C-H. In this study, the O-H bond lengths also are lesser than the C-H ones. The O-H bond lengths vary from 0.9925 to 0.9936 Å and from 0.8531 to 0.8441 Å by B3LYP and HF methods, respectively. The asymmetry of the benzene ring is also evident from the positive deviation of C1–C2–Cl9 and C3–C2–Cl9 are inversely arranged like experimental, B3LYP and HF and reverse in that other angle (C3–C2–Cl9). The C2-C3-Cl10 calculated values are greater than the C4-C3-Cl10. The angles C4-C5-Cl11 and C6-C5-Cl11 are around the value approximatively 119° in both B3LYP and HF methods. C2–C1–C6 is highest value of the angle in both the HF and B3LYP and experimental methods.

**4.3. Thermodynamic Properties**

The values of thermodynamic parameters of 235TCBP at 298.15 K in ground state are listed in Table 2. The statically thermodynamic functions: heat capacity (C), entropy (S), and enthalpy changes (H) for the title molecule were obtained from the theoretical harmonic frequencies and listed in Table 4. From the Table 4, it can be observed that these thermodynamic functions are increasing with temperature between from 100 to 1000 K [11]. In this enthalpy is having the lowest value in comparison with heat capacity and entropy. Similarly, the entropy having the higher most value. The correlation equations between heat capacity, entropy, enthalpy changes and temperatures were fitted by quadratic formulas and the corresponding fitting factor ($R^2$) for these thermodynamic properties is determined. The correlation factor for enthalpy is grater in comparison with other two. The corresponding fitting equations are as follows and the correlation graphics of

that show in Figs. 3.

$$C = -6.0763 + 0.10261T - 5.07833x10^{-5}T^2 \quad (R^2 = 0.99151)$$

$$S = 56.3481 + 0.14307T - 4.4799x10^{-4}T^2 \quad (R^2 = 0.99792)$$

$$H = -1.91559 + 0.0231T + 2.20533x10^{-5}T^2 \quad (R^2 = 0.99838)$$

Heat capacity is at the final end slightly decreases with other two. All the thermodynamic data supply helpful information for the further study on the 235TCBP. They can be used to compute the other thermodynamic energies according to relationships of thermodynamic functions and estimate directions of chemical reactions according to the second law of thermodynamics in Thermochemical field.

**4.4. Atomic charges**

Atomic charge is calculated an essential role in the application of quantum chemical application to molecular system because of atomic charges effect. The atomic charge distributions over the atoms suggest the formation of positive and negative pairs giving the charge transfer in the molecule. The atomic population analysis in 235TCBP molecule was calculated using B3LYP and HF levels with 6-311++G(d,p) basis sets and are listed in Table 4 and are shown in the Fig 4. The results show that substitution of the aromatic ring by Cl and OH group of atoms leads to a redistribution of electron density. The charge changes with basis set presumably occurs due to polarization. For example, the charges of Cl are equal and almost same negative charge in B3LYP and HF methods. Hydrogen in the OH group is having highest positive charge among all the hydrogen atoms. O atom is having the value of highest negative value among all the atoms and the value is 0.301188 and 0.338783 in B3LYP and HF. The charge distribution of 235TCBP (Fig. 6) shows the carbon atomic charges for the compounds were found to be both positive and negative at the basis set. The Cl and OH group in the molecule accepted the electrons.

**4.5. Frontier molecular orbitals (FMOs)**

The FMO play an important role in the optical and electric properties, as well as in quantum chemistry and UV–Vis. spectra [12]. Gauss-Sum 2.2 Program [13] was used to calculate group contributions to the molecular orbitals (HOMO and LUMO). The HOMO indicates the power to donate an electron, LUMO as an electron acceptor indicates the ability to obtain an electron. The HOMO and LUMO determines the kinetic stability, chemical reactivity and, optical polarizability and chemical hardness–softness of a molecule.

In order to evaluate the energetic behavior of the title compound, we carried out calculations in DMSO, acetone and chloroform phase. The energies of four important molecular orbitals of 235TCBP: the second highest and highest occupied MO's (HOMO and HOMO−1), the lowest and the second lowest unoccupied MO's (LUMO and LUMO+1) were calculated using B3LYP/6-311++G(d,p). 3D plots of the HOMO-1, HOMO, LUMO and LUMO+1 orbitals computed at the B3LYP/6-311G++(d,p) level for 235TCBP molecule (in gas phase) are illustrated in Fig. 5. It is clear from the figure that, while the HOMO is localized on almost the whole molecule, LUMO is especially localized on the ring. Both the HOMOs and the LUMOs are mostly -anti-bonding type orbitals. The calculated energy values of the HOMO are -6.6925, -6.6925 and -6.6949 eV in DMSO, acetone and chloroform, respectively. Similarly, the LUMO energy values are -1.2659, -1.2697

and -1.2919 eV. The energy gap between HOMO and LUMO indicates the molecular chemical stability. In this molecule, the value of energy separation between the HOMO and LUMO are -5.4265, -5.4227 and -5.4029 eV in DMSO, acetone and chloroform, respectively. The major contributions of the transitions were designated with the aid of SWizard program [14]. In view of calculated absorption spectra, the maximum absorption wavelength corresponds to the electronic transition from the HOMO to LUMO.

**4.6. Ultraviolet spectra analysis**

Ultraviolet spectra analyses of 235TCBP have been investigated in DMSO chloroform and gas phase by theoretical calculation. On the basis of fully optimized ground-state structure, TD-DFT/B3LYP/6-311++G(d,p) calculations have been used to determine the low-lying excited states of 235TCBP. The theoretical electronic excitation energies, oscillator strengths and absorption wavelength are also listed in Table 5 and the UV graph of solvents are shown in the Fig 6. Calculations of the molecular orbital geometry show that the absorption maxima of this molecule correspond to the electron transition between frontier orbitals such as translation from HOMO to LUMO. As can be seen from Table 5, the calculated absorption maxima values have been found to be 263.78, 241.26, 226.98, 217.28, 213.82, 207.87 and 198.36 nm for DMSO, 263.79, 241.26, 226.90, 217.64, 213.76, 213.76 2507.80 and 198.63 nm for acetone , 264.87, 241.37, 227.50, 220.14, 213.51, 207.53 and 199.98 nm for chloroform at DFT/B3LYP/6-311++G(d,p) method. In all three, chloroform is slightly increase in value. But the iterations are doing for three solvents and two peaks are visible and one peak is dim manner. In these remaining peaks are invisible and oscillator strength also very feeble 0.0001. It is seen from Table 5, calculations performed at DMSO, acetone and chloroform are close to each other when compared with each other.

**4.7. Electrostatic potential, total electron density and molecular electrostatic potential**

In the present study, the electrostatic potential (ESP) and molecular electrostatic potential (MEP) of 235TCBP are illustrated in Fig. 7. The MEP which is a plot of electrostatic potential mapped onto the constant electron density surface. The MEP is a very necessary in identifying the electrophile will be attracted to negative regions. In the majority of the MEP, while the maximum negative region which preferred site for electrophilic attack indications as red colour and the maximum positive region which preferred site for nucleophilic attack symptoms as blue colour. The importance of MEP simultaneously displays molecular size, shape as well as positive, negative and neutral electrostatic potential regions in terms of colour grading (Fig. 7) and is very useful in research of molecular structure with its physiochemical property relationship [15-17].

The different values of the electrostatic potential at the MEP surface are represented by different colors; red, blue and green represent the regions of most negative, most positive and zero electrostatic potential, respectively. In all the three chlorine atoms the color is light greenish yellow color and potential -0.01267 and -0.0072. The oxygen atom is negative potential about -0.0021. The deepest blue color is in between the two hydrogen atoms and it indicates positive potential around the hydrogen atoms (H7 and H13). The color code of these maps is in the range between -0.07763 a.u. (deepest red) to 0.07763 a.u. (deepest blue) in

compound, where blue indicates the strongest attraction and red indicates the strongest repulsion. ESP map is having the value around -0.008375 to +0.008375 a.u. The oxygen atoms of ESP is having the value -0.00039 a.u. As can be seen from the MEP map of the title molecule, while regions having the positive potential are over the hydrogen atoms, the regions having the negative potential are over the electronegative (Cl and OH) atoms.

### 4.8. Vibrational analysis

The maximum number of potentially active observable fundamentals of a non-linear molecule which contains N atoms is equal to (3N-6), apart from three translational and three rotational degrees of freedom. Hence, 235TCBP molecule, that was planar, has 13 atoms with 33 normal modes of vibrations. All vibrations are active both in Raman and infrared absorption. The detailed vibrational assignment of the experimental wavenumbers is based on normal mode analyses and a comparison with theoretically scaled wavenumbers by B3LYP and HF methods. The observed and simulated infrared and Raman spectra of 235TCBP is shown in Figs. 8-9, respectively. The observed and scaled theoretical frequencies using HF and DFT (B3LYP) with 6-311++G(d,p) basis sets with PEDs are listed in Table 6.

#### 4.8.1. C-H vibrations

The aromatic C–H stretching vibrations in tetra substituted benzene rings are generally observed in the region 3000–3100 $cm^{-1}$ [18]. They are having only two vibrations and that must be medium and weak vibrations. The medium and weak band is observed at 3080 and 3050 $cm^{-1}$ in FTIR and FT-Raman can be assigned to C-H stretching with PEDs 98% and 99%, respectively. The aromatic CH stretching band is found to be weak and this is due to the decrease of dipole moment caused by the reduction of negative charge on the carbon atom. This reduction occurs because of the electron withdrawal on the carbon atom by the substituent due to the decrease of inductive effect. The corresponding calculated fundamentals using B3LYP/6-311++G(d,p) are 3078 and 3046 $cm^{-1}$. These deviations have been reduced by the scaling procedure and scaled wave numbers.

The bands due to C–H in-plane bending vibrations are observed in the region 1000–1300 $cm^{-1}$[19,20]. For this compound, the C–H in-plane bending vibrations were observed at 1120 and 1070 $cm^{-1}$ in FT-IR. The PED of vibrations shows that they are not in pure modes. The theoretically scaled vibrations by B3LYP/6-311++G(d,p) level method also shows good agreement with experimentally recorded data. The C–H out-of-plane bending vibrations appear within the region 900–675 $cm^{-1}$. But they the vibration identified at 615 $cm^{-1}$ a strong band is observed in FT-Raman are assigned to C–H out-of-plane bending for 235TCBP. The value is slightly deviating from the region indicates that only two hydrogen in this region. After scaling procedure, the theoretical C–H vibrations are in slightly higher values with the experimental values and literature.

### 4.8.2. Ring vibrations

The ring stretching vibrations are significant in spectrum analysis of benzene and its derivatives. The C=C and C-C stretching vibrations, known as semicircle stretching usually occur in the region 1400–1625 $cm^{-1}$ [21, 22]. The C=C stretching vibrations of the present compound are strongly observed at 1595, 1570 and 1475 $cm^{-1}$. These assignments are in line with the literature. The C-C stretching vibrations were observed at 1375, 1300 and 1275 $cm^{-1}$. When compared to the literature range cited above, there is a considerable decrease in frequencies which is also worsening with the increase of mass of substitutions.

In the present work, three bands present at 875 and 820 $cm^{-1}$ assigned to CCC in-plane bending and 560 and 460 $cm^{-1}$ supplementary bands assigned to CCC out-of-plane bending. These assignments are in line with the assignments proposed by the literature. The theoretically computed values by B3LYP/6-311++G(d,p) method for CCC out-of-plane bending are shown in the table 6.

### 4.8.3 C-Cl vibrations

The vibrations belonging to C-X (X=F, Cl, Br.....) bonds which are formed between the ring and the halogen atoms, are interesting since mixing of vibrations are possible due to the lowering of molecular symmetry and the presence of heavy atoms [23-26]. In Raman spectra, the vibration bands result in strong bands for Cl, Br and I atoms, but for F the bands are weaker. According to these early reports, the C–Cl stretching band is expected around 505–380 $cm^{-1}$. In FT-Raman spectrum of 235TCBP, a strong band at 330 and 302 $cm^{-1}$ is assigned to C-Cl stretching vibration. The theoretical wavenumber of C-Cl stretching vibration 327 and 304 $cm^{-1}$ by B3LYP/6-311++G(d,p) coincides very well with the experimental value. The PED corresponding to C-Cl stretching vibration is 43 and 46 %. The C-Cl in-plane bending vibrations are assigned to the Raman bands at 230 and 202 $cm^{-1}$ and 180 in out-of-plane bending respectively. After scaled up computed these values for C–Cl in-plane and out-of-plane bending vibrations by B3LYP/6-311++G(d,p) method nearly coincides with experimental values.

### 4.8.4. O-H vibrations

The OH group gives rise to three vibrations, stretching, in-plane bending and out-of-plane bending vibrations. The OH group vibrations are likely to be the most sensitive to the environment, so they show pronounced shifts in the spectra of the hydrogen-bonded species. The O–H stretching band is characterized by very broad band appearing near about 3400–3600 $cm^{-1}$. The hydroxyl stretching vibrations are generally observed in the region around 3500 $cm^{-1}$ [ 27, 28]. In our case a weak band in FT-IR spectrum at 3525 vw $cm^{-1}$ is assigned to OH stretching vibration. The calculated value by B3LYP/6-311G++(d,p) level show at 3670 $cm^{-1}$. It is true from PED value contributing to 100%, suggested pure stretching mode, as shown in Table 9. The in-plane and out-of-plane bending vibrations are observed at 1165 $cm^{-1}$ and no out-of-plane bending vibrations. The theoretically scaled vibrations by B3LYP/6-311++G(d,p) level method also shows good agreement with experimentally recorded data.

**4.10. Hirshfeld surface analysis**

The Hirshfeld surface analysis of was performed with the Crystal Explorer 3.1 program [ 29] using the experimental structure as input to reveal the inter molecular interactions in the crystal. The results are presented in Fig. 11 and Fig. 12, which represent the 3D Hirshfeld surface (dnorm) and 2D fingerprint histogram of the molecule, respectively. In Fig. 11, the red colored points represent the intermolecular contacts shorter than the sum of their van der Waals radii (hydrogen bonds) while contacts greater than this sum are blue color and green colors represent contacts around the sum of the van der Waals radii.The oxygen region is having the red color points and chlorine is having green color. The dnorm values were determined to be in the range -0.556 (negative points-red) to 1.502 (positive points-blue) Å and di values were determined to be in the range 0.776 to 2.716, its mean value is 1.802 Å. The de, shape index, and curvedness mean value are 1.805, 0.229 and -0.990 Å and 2D fingerprint histograms shown in Fig. 4 (a-d) indicate the contributions of the intermolecular contacts to the Hirshfeld surfaces to be all, C..C (1.7%), C..H (3.6%) and Cl..C (13.6%).

**4.11. NMR spectra and calculations**

The isotropic chemical shifts are often used to anticipate and interpret the structure of large molecular systems. Additionally, the combined use of NMR and calculated methods acting an opportunity to obtain more exact results. The structure in the title compound (DBQA) was confirmed with the help of $^{1}H$ NMR and $^{13}C$ NMR spectral study. The theoretical $^{1}H$ and $^{13}C$ NMR chemical shifts have been compared with the experimental data as shown in Table 7. Chemical shifts are reported in ppm relative to TMS for $^{1}H$ and $^{13}C$ NMR spectra. The atom statues were numbered according to Fig. 13. Then, gauge-including atomic orbital (GIAO) 1H and 13C chemical shift calculations of the compound was made by the same method using 6-311++G(d,p) basis set IEFPCM/CDCl3 solution. Aromatic carbons give signals in theoretical data 165.5, 152.6, 148.4, 139.3, 135.8 and 128.5 ppm for C6, C2, C4, C3, C5 and C1. The experimental data three only C6, C3 and C1 are slightly coincide with the theoretical one. But for the aromatic hydrogen atoms only two is almost equal. The hydrogen atom attached to the O-H in group is having the value experimental 5.7 ppm and theoretical value is 5.6 ppm.

**4.12. Molecular docking analysis:**

AutoDock is a suite of automated docking tool. It is designed to predict how small molecules, such as substrates or drug candidates, bind to a receptor of known 3D structure and molecular docking is shown in the Fig .14 [30, 31]. The protein add with Kollmann charges were assigned. Through which hydrogens were added, side chains were optimized for hydrogen bonding. The energy minimized protein was then saved in PDB format. The MGLTools-1.4.6 is used nonpolar hydrogens were merged, AutoDock atom type AD4 and Gasteiger charges were assigned and finally saved in protein. pdbqt format. The active site of the protein is the binding site or usually a pocket at the surface of the protein that contains residues responsible for substrate specificity which often act as proton donors or acceptors. Identification and characterisation of binding site are the key step in structure-based drug design. The binding site has been

identified by computational and literature reports. Grid parameter files (protein.gpf) and docking parameter files (ligand.dpf) have written using MGLTools-1.4.6. Receptor grids were generated using 84x86x84 grid points in xyz with grid spacing of 0.375 Å. Grid box was centered co crystallized ligand map types were generated using autogrid4. Docking of macromolecule was performed using an empirical free energy function. Results differing by 2.0 Å in positional root-mean square deviation (RMSD) were clustered together and represented by the result with the most favourable free energy of binding. The title molecule residues VAL 54 and SER 2 were involved in interactions with title molecule in the active site of Protein. The length of hydrogen bonds formed 2.1 and 1.9 Å. The free and internal energies are associated with atom -1368.67 and -4.43 kcal/mol at Temperature, T = 298.15 K

## 5. Conclusion

The molecular geometry is obtained by second potential energy scan 2 curve with dihedral angle C1-C6-O12-H13 the link between the same two groups in the moecule. The C-O bond length is lighter in experimental in comparison than the theoretical one. The O-H bond length shows a considerable diminish when substituted in place of C-H. Heat capacity is at the final somewhat decreases with other entropy and enthalpy. Hydrogen in the oxygen-hydrogen group is having maximum positive charge among all the hydrogen atoms. In this molecule, the value of energy separation between the HOMO and LUMO are in DMSO, acetone and chloroform, respectively. In all three, chloroform is slightly increase in value. MEP map is having the positive potential are over the hydrogen atoms, the regions having the negative potential are over the electronegative atoms. The theoretical C–H vibrations are in somewhat higher values with the experimental values and literature. The C–Cl in-plane and out-of-plane bending vibrations are coincided with experimental values. The molecule is having two non-polar hydrogens, six aromatic carbon atoms and one totable bond. The hydrogen atom committed to the O-H in group is having the value experimental 5.7 ppm and calculated value is 5.6 ppm. Molecular AutoDock is used in to find the free, internal energies and hydrogen atoms bond distances.

**References**


[1] Z.Sun, X.Ma, X. Hu, Environmental Science and Pollution Research, volume 24, (2017) 14355–14364

[2] G.S. Pozan, I.Boz Environmental Engineering ScienceVol. 25( 2008)

[3] P. Jin, S.K. Bhattacharya, Journal of Environmental Engineering, Volume 122 (1996)

[4] H. Juha A. Apajalahti , S.Mirja, Salkinoja-Salonen, Applied Microbiology and Biotechnology volume 25, pages 62–67(1986)

[5] W.F.Jardim, S.G.Moraes, M.M.K.Takiyama, Toxicity of intermediates, Volume 31,(1997) 1728-1732

[6] Thiruvalluvar, M. Subramanyam, R. J. Butcher, Prakash Karegoudar and B. Shivarama Holla, Acta crystallographica Section E E64, o60-066

[7] Frisch M J, Gaussion 09 Program, Gaussian, Inc., Wallingford, CT, 2004.

[8] Karabacak M, Kurt M, Spectrochim. Acta A 71 (2008) 876-883.

[9] Jamróz M H, Vibrational Energy Distribution Analysis, VEDA 4, Warsaw, 2004.

[10] Dennington R I, Keith T, Millam J, Eppinnett K, W. Hovell, Gauss View Version

[11] J Bevan Ott, J. Boerio-Goates, Calculations from Statistical Thermodynamics, Academic Press, 2000.

[12] I. Fleming, Frontier Orbitals and Organic Chemical Reactions, Wiley, London, 1976.

[13] N.M.O' Boyle, A.L.tenderholt, K.M.langer, A Library for package-independent computational chemistry algorithms.J.Comput.Chem. 29(2008) 839-845.

[14] S.I. Gorelsky, SWizard Program Revision 4.5, http://www.sg.chem.net/, University of Ottawa, Ottawa, Canada, 2010.

[15] I. Alkorta, J.J. Perez, Int. J. Quant. Chem. 57 (1996) 123-135.

[16] E. Scrocco, J. Tomasi, in: P. Lowdin (Ed.), Advances in Quantum Chemistry, 402 Academic Press, NewYork, 1978. 403.

[17] F.J. Luque, M. Orozco, P.K. Bhadane, S.R. Gadre, J. Phys. Chem. 97 (1993) 9380-9384.

[18] N.P. Singh, R.V. Yadav. Indian J. Phys. B, 75 4 (2001) 347-355.

[19] G.Varsanyi, Vibrational Spectra of Benzene Derivatives, Academic Press, New York, 1969.

[20] M.H. Jamroz, J.Cz. Dobrowolski, R. Brzozowski, J. Mol. Struct. 787 (2006) 172-183.

[21] A. Altun, K. Gölcük, M. Kumru, J. Mol. Struct. (Theochem.) 625 (2003) 17-24.

[22] V. Krishnakumar, R.J. Xavier. Indian J. Pure. Appl. Phys., 41 (2003) 95–98.

[23] M. Rogojerova, G. Kereszturyb, B. Jordanova, Spectrochim. Acta A 61 (2005) 1661-1670.

[24] C.S. Hiremath, J. Yenagi , J. Tonannavar, Spectrochim. Acta A 68 (2007) 710-717.

[25] V. Arjunan, I. Saravanan, P. Ravindran, S. Mohan, Spectrochim. Acta A 74 (2009) 642-649.

[26] V. Sortur, J. Yenagi, J. Tonannavar, V.B. Jadhav , M.V. Kulkarni , Spectrochim. Acta A 71 (2008) 688-694.

[27] D. Michalska, D.C. Dienko, A.J. Abkowicz-Bienko and Z. Latajka. J. Phys. Chem., 100 (1996) 123-

129.

[28] D. Sajan, I. Hubert Joe, V.S. Jayakumar, J. Zaleski, J. Mol. Struct. 785 (2006) 43–53.

[29] M. Turner, J. McKinnon, S. Wolff, D. Grimwood, P. Spackman, D. Jayatilaka, M. 539 Spackman, CrystalExplorer17, University of Western Australia Crawley, Western Australia, 540 Australia, 2017.

[30] P. Manjusha, Johanan Christian Prasana, S. Muthu, B. Fathima Rizwana, Chem. Data.Coll. 20 (2019) 100191.

[31] BR. Raajaraman, N.R. Sheela, S. Muthu, J. Mol. Struct. 1188, (2019) 99-109.

Fig .1 Potential energy scan of 235TCBP

Fig .2 Optimized geometry of 235TCBP

Fig .3 Correlation graph of thermodynamic functions of 235TCBP

Fig .4 Atomic charge analysis of 235TCBP

Fig .5 HOMO-1, HOMO, LUMO and LUMO+1 of 235TCBP

Fig .6 UV graph of 235TCBP

Fig .7 Molecular electrostatic potential (MEP) and electro static potential of 235TCBP

Fig .8 Observed and simulated infrared spectra of 235TCBP

Fig .9 Observed and simulated spectra of 235TCBP

Fig .10 Hirshfeld surface analysis of 235TCBP

Fig .11 Hirshfeld charge analysis of 235TCBP

Fig .12 NMR analysis of 235TCBP

Fig.13 Molecular docking study 235TCBP

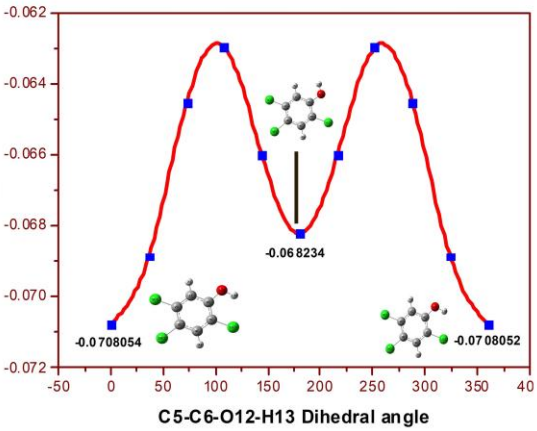
-0.062
-0.064
-0.066
-0.068
-0.070
-0.072
-50
0
50
100
150
200
250
300
350
40
-0.068234
-0.0708054
-0.0708052
C5-C6-O12-H13 Dihedral angle

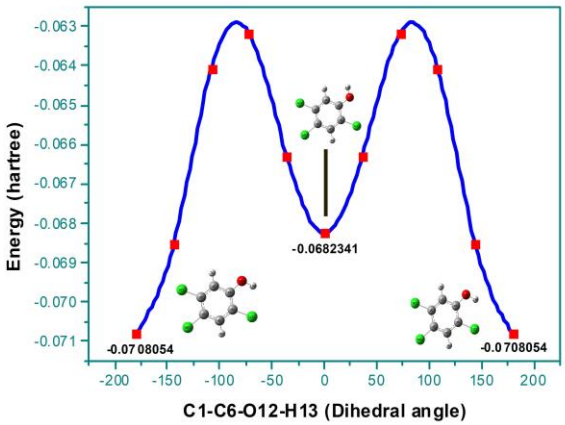
Energy (hartree)
-0.063
-0.064
-0.065
-0.066
-0.067
-0.068
-0.069
-0.070
-0.071
-200
-150
-100
-50
0
50
100
150
200
-0.0682341
-0.0708054
-0.0708054
C1-C6-O12-H13 (Dihedral angle)

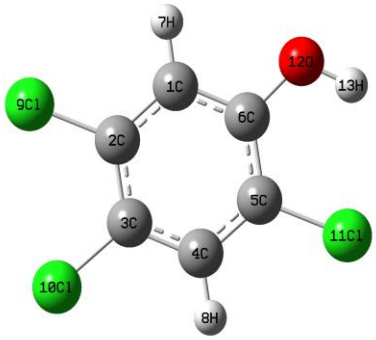
7H
12O
13H
1C
9Cl
6C
2C
5C
3C
11Cl
4C
10Cl
8H

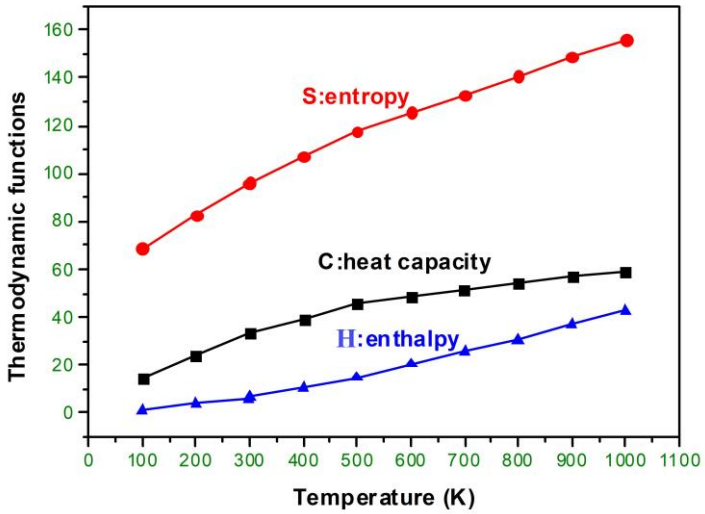
Thermodynamic functions
Temperature (K)
S:entropy
C:heat capacity
H:enthalpy
0
20
40
60
80
100
120
140
160
0
100
200
300
400
500
600
700
800
900
1000
1100

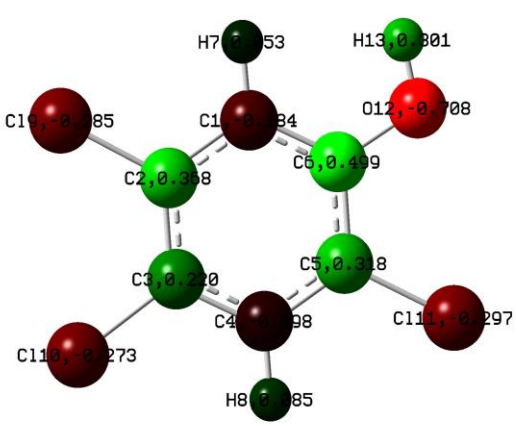
H7
H13,0.301
O12,-0.708
C2,0.308
C6,0.499
C5,0.348
C11,-0.297
H8

B3LYP

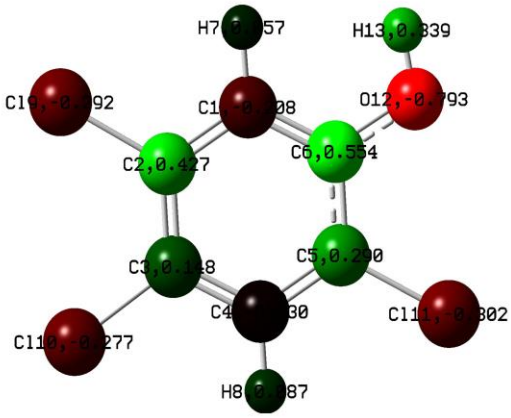
H7
H13,0.339
O12,-0.793
C2,0.427
C6,0.554
C5,0.290
C11,-0.302
H8

HF

**HOMO= -9.8268 eV**

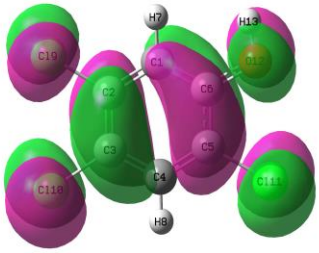


**HOMO-1 = -10.4763 eV**

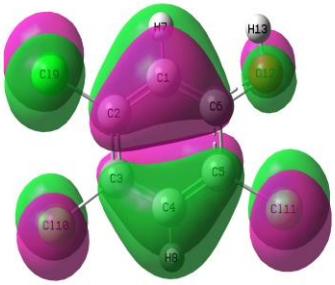


**LUMO = -1.0112 eV**

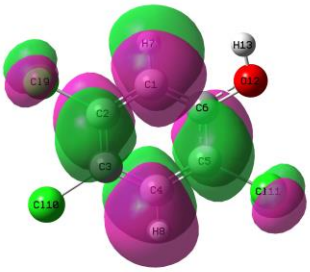


**LUMO+1 = -0.8165 eV**

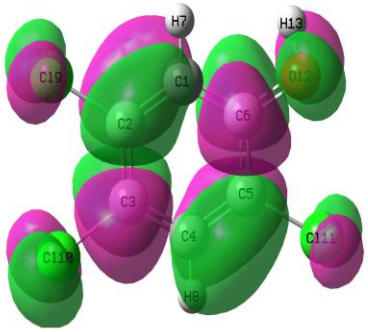


**HOMO - LUMO = 8.8156 eV**

**HOMO-1 - LUMO+1 = 9.6598 eV**

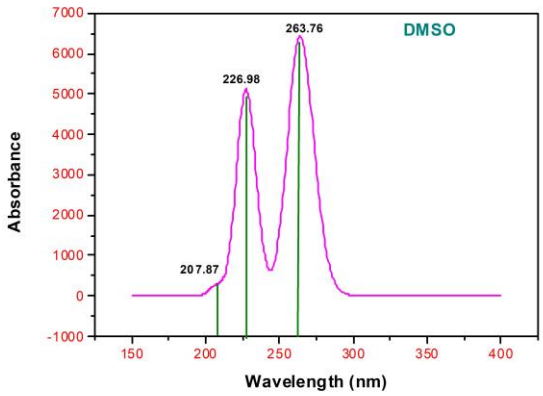
DMSO
263.76
226.98
207.87
Absorbance
Wavelength (nm)

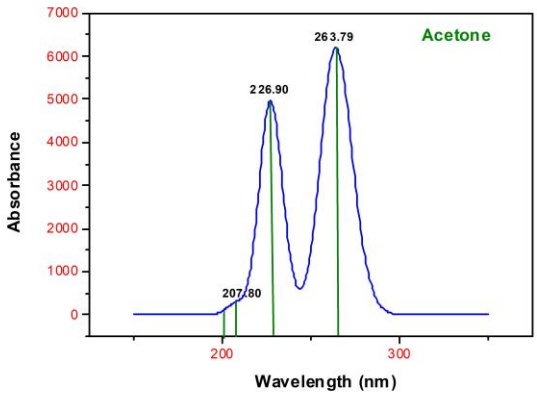
Acetone
263.79
226.90
207.80
Absorbance
Wavelength (nm)

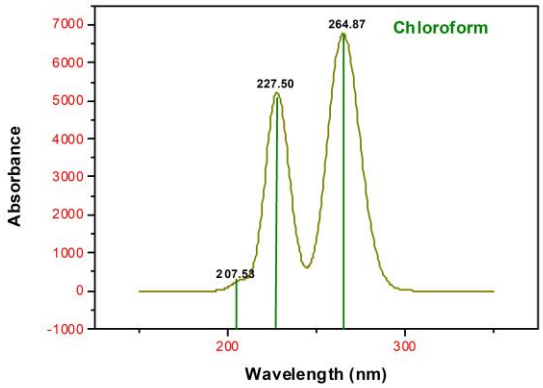
Chloroform
264.87
227.50
207.58
Absorbance
Wavelength (nm)

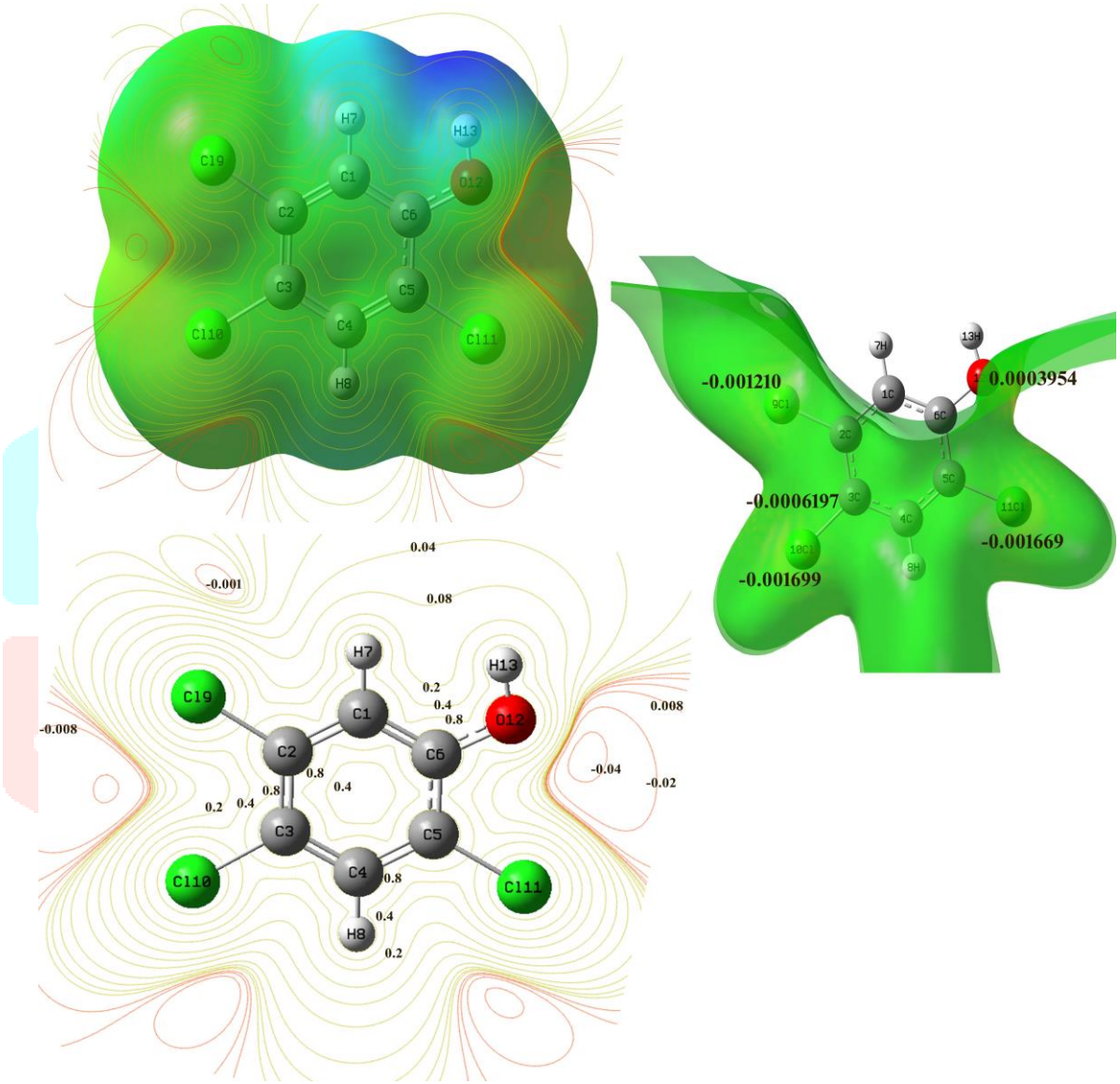
H7
H13
C19
C1
O12
C2
C6
C3
C5
C110
C4
C111
H8
-0.001210
0.0003954
-0.0006197
-0.001669
-0.001699
0.04
-0.001
0.08
0.2
0.4
0.8
0.008
-0.008
-0.04
-0.02

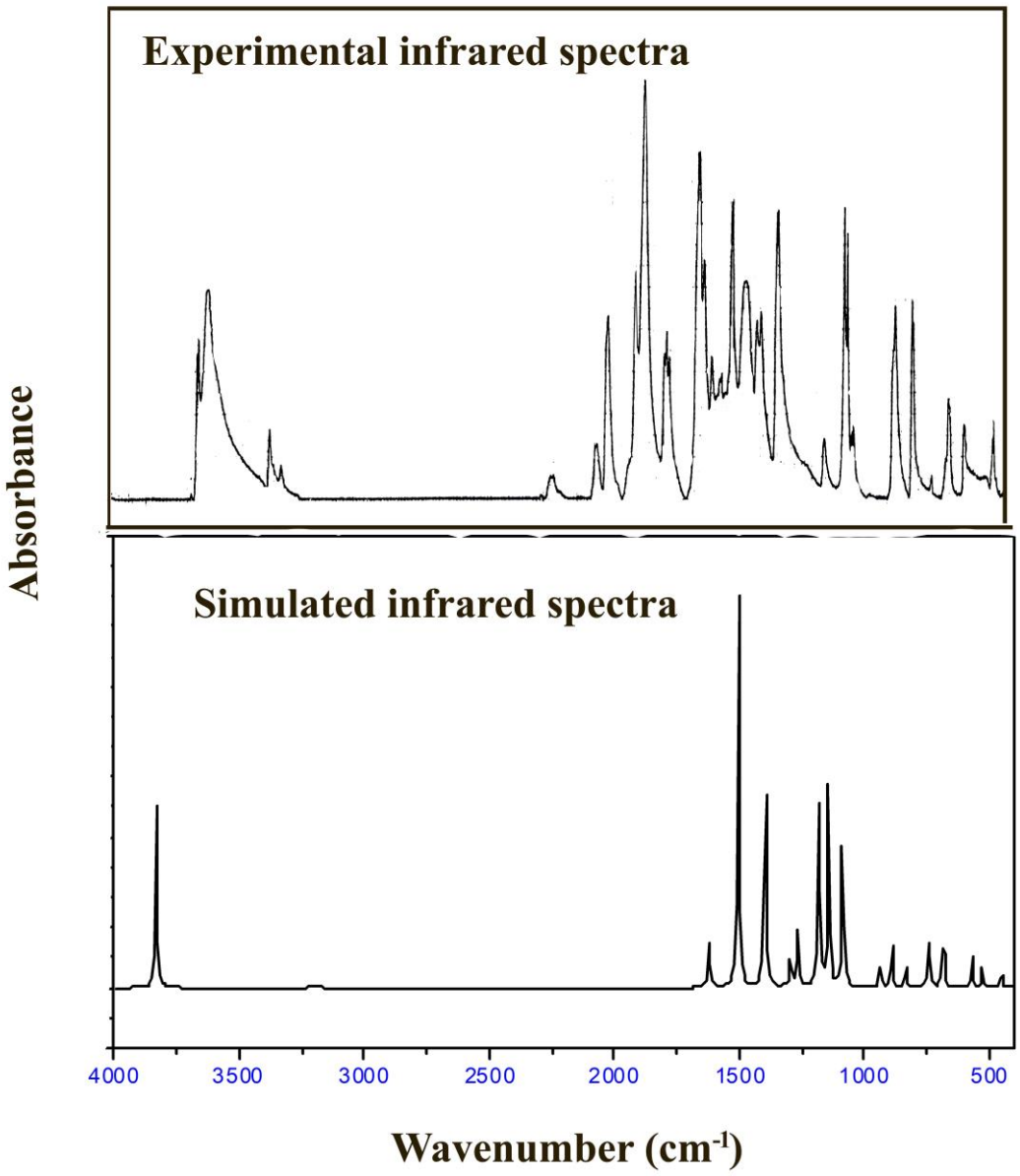
Experimental infrared spectra
Simulated infrared spectra
Absorbance
4000
3500
3000
2500
2000
1500
1000
500
Wavenumber (cm-1)

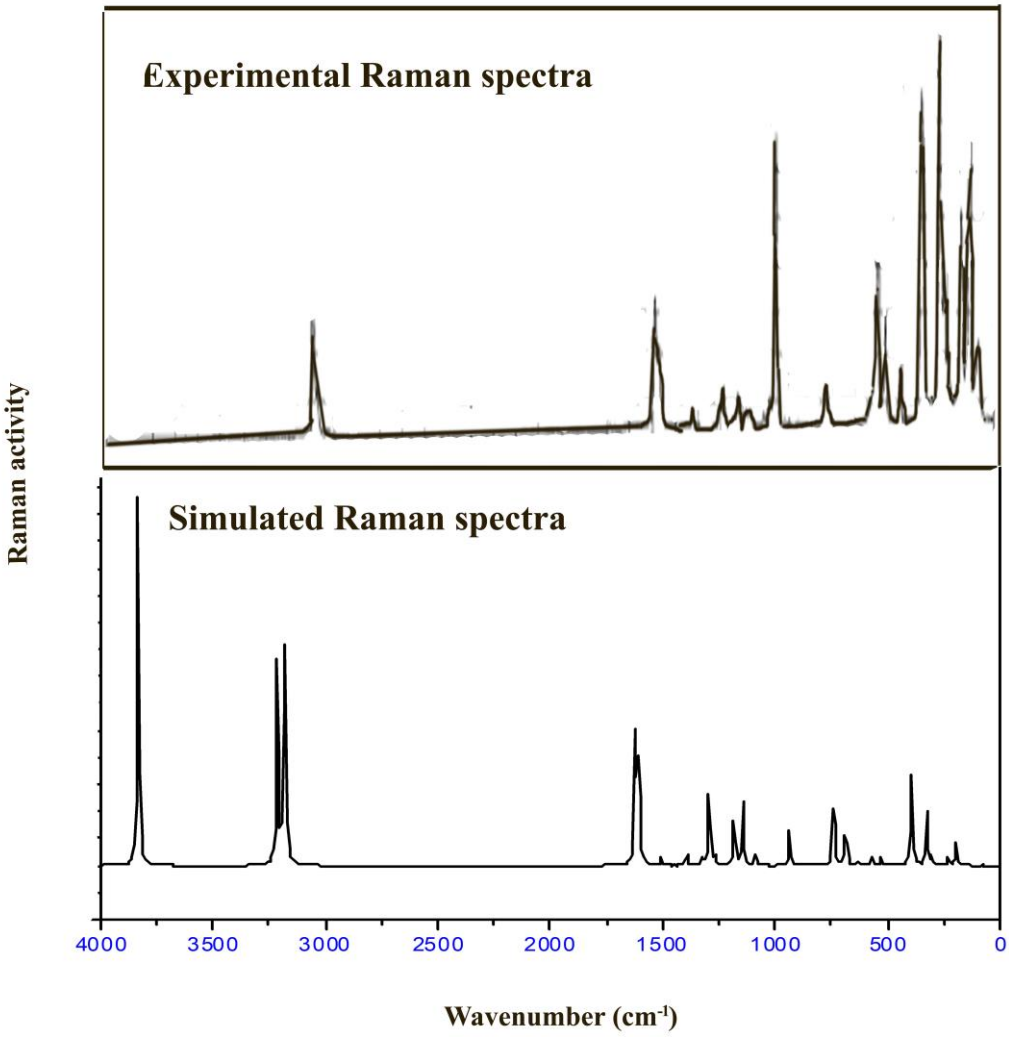
Experimental Raman spectra
Simulated Raman spectra
Raman activity
4000
3500
3000
2500
2000
1500
1000
500
0
Wavenumber (cm-1)

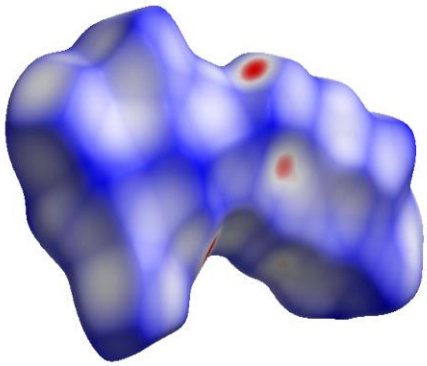

dnomal=0.440

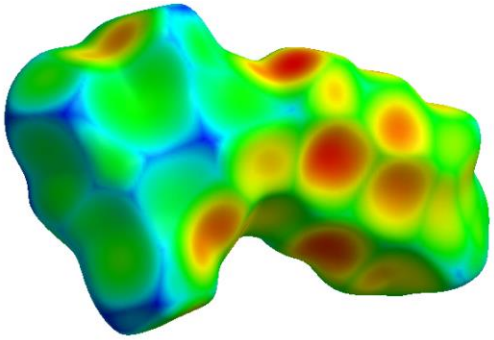

de=1.835

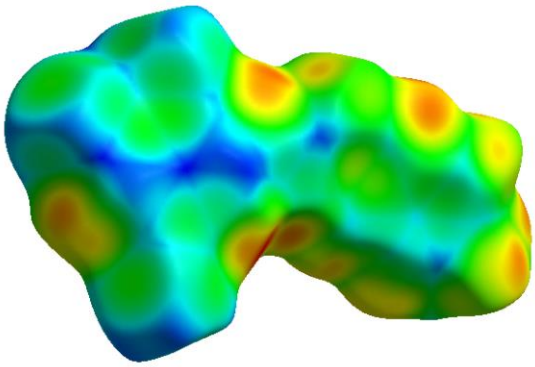

di=1.819

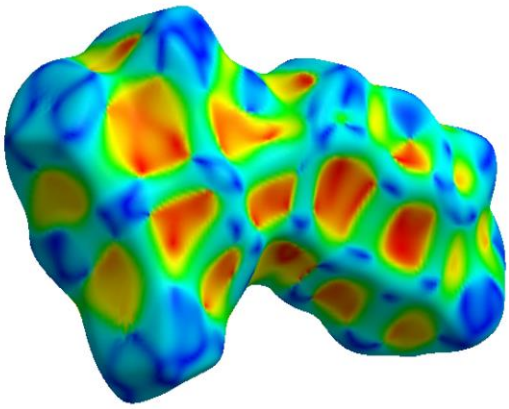

shape index=0.258

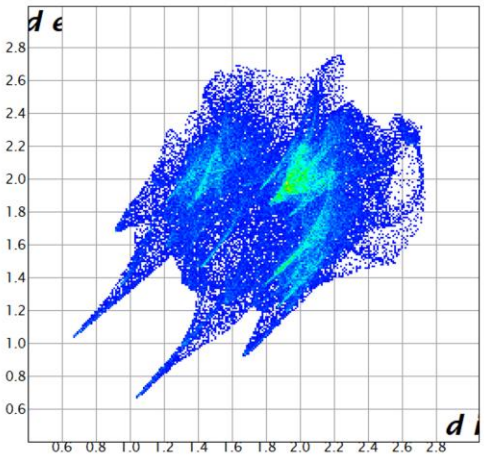

All

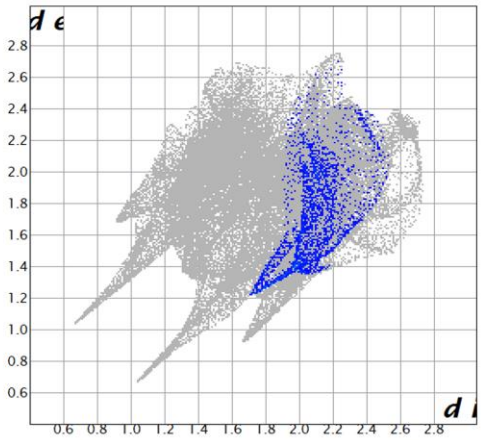

C..H.. 3.6%

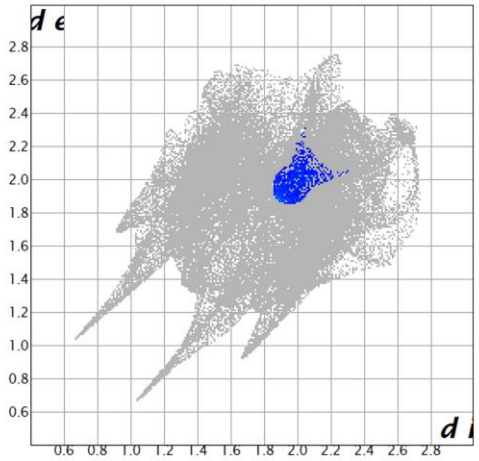

C..C.. 1.7 %

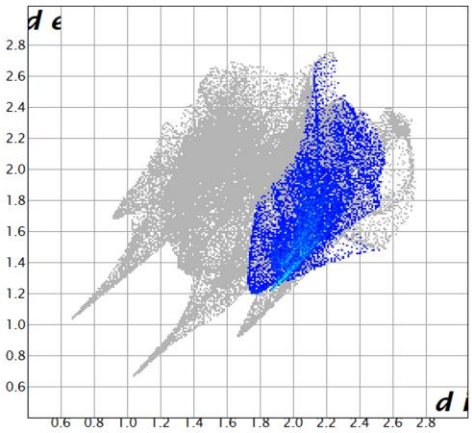

Cl..H.. 13.6 %

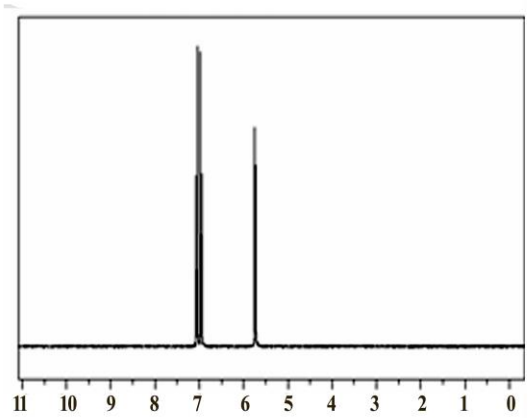


Experimental Proton NMR

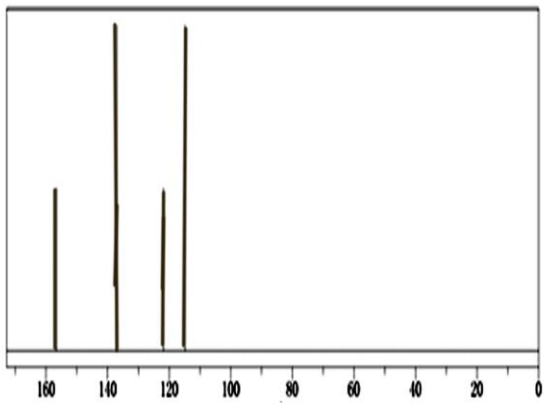


Experimental Carbon NMR

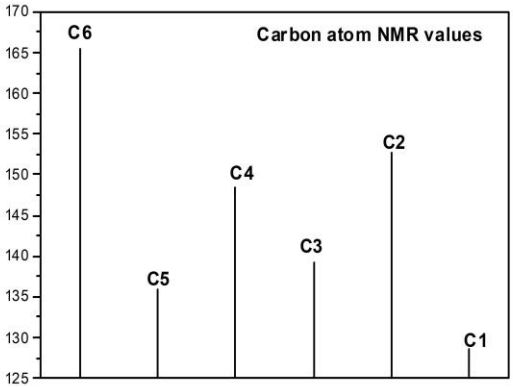


Carbon atoms NMR

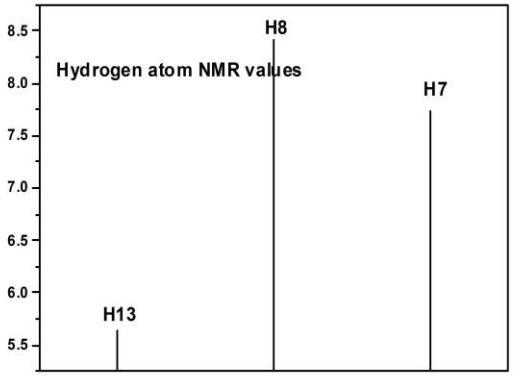


Hydrogen atom NMR

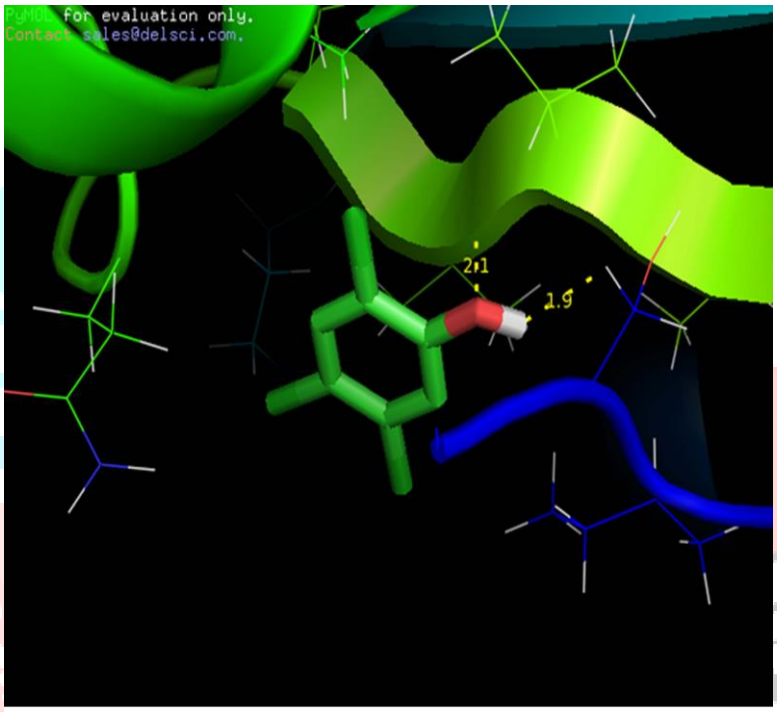


**Molecular docking**

Table 1. The scan values of 235TCBP

| Scan 1 | | Scan2 | |
|---|---|---|---|
| Degree | Value | Degree | Value |
| 180 | -0.0708 | 0 | -0.0708 |
| -144 | -0.0685 | 36 | -0.0689 |
| -108 | -0.0641 | 72 | -0.0646 |
| -72 | -0.0632 | 108 | -0.0630 |
| -36 | -0.0663 | 144 | -0.0660 |
| 0 | -0.0682 | 180 | -0.0682 |
| 36 | -0.0663 | 216 | -0.0660 |
| 72 | -0.0632 | 252 | -0.0630 |
| 108 | -0.0641 | 288 | -0.0646 |
| 144 | -0.0685 | 324 | -0.0689 |
| 180 | -0.0708 | 360 | -0.0708 |

Table 2. Optimized parameters of 235TCBP

| Bond length | B3LYP | HF | Expeiment[a] |
|---|---|---|---|
| C1-C2 | 1.393 | 1.385 | 1.404 |
| C1-C6 | 1.393 | 1.382 | 1.396 |
| C1-H7 | 1.084 | 1.075 | |
| C2-C3 | 1.396 | 1.382 | 1.385 |
| C2-Cl9 | 1.745 | 1.732 | 1.731 |
| C3-C4 | 1.394 | 1.385 | 1.388 |
| C3-Cl10 | 1.746 | 1.734 | 1.730 |
| C4-C5 | 1.387 | 1.376 | 1.370 |
| C4-H8 | 1.082 | 1.072 | |
| C5-C6 | 1.402 | 1.390 | 1.398 |
| C5-Cl11 | 1.745 | 1.733 | 1.749 |
| C6-O12 | 1.357 | 1.339 | 1.226 |
| O12-H13 | 0.963 | 0.941 | |
| Bond angle | | | |
| C2-C1-C6 | 121.003 | 120.958 | 119.600 |
| C2-C1-H7 | 119.057 | 119.095 | |
| C6-C1-H7 | 119.940 | 119.947 | |
| C1-C2-C3 | 119.916 | 120.025 | 120.000 |
| C1-C2-Cl9 | 118.433 | 118.081 | 120.000 |
| C3-C2-Cl9 | 121.651 | 121.894 | 120.400 |
| C2-C3-C4 | 119.305 | 119.124 | 117.200 |
| C2-C3-Cl10 | 121.877 | 122.287 | |
| C4-C3-Cl10 | 118.818 | 118.589 | |
| C3-C4-C5 | 120.692 | 120.881 | 118.300 |
| C3-C4-H8 | 119.645 | 119.552 | |
| C5-C4-H8 | 119.663 | 119.567 | |
| C4-C5-C6 | 120.354 | 120.226 | 119.900 |
| C4-C5-Cl11 | 119.803 | 119.578 | |
| C6-C5-Cl11 | 119.843 | 119.196 | |
| C1-C6-C5 | 118.730 | 118.786 | 119.600 |
| C1-C6-O12 | 122.780 | 122.441 | |
| C5-C6-O12 | 118.491 | 118.773 | |

a[6]

Table 3. Thermodynamic properties at different temperatures at the B3LYP/6-311++G(d,p) level of 235TCBP

| Temperature | $C_V$ | S | E |
|---|---|---|---|
| 100 | 14.534 | 68.971 | 1.069 |
| 200 | 24.055 | 82.763 | 4.026 |
| 298.15 | 33.375 | 95.908 | 6.085 |
| 300 | 33.512 | 96.364 | 6.576 |
| 400 | 39.516 | 107.202 | 10.508 |
| 500 | 45.788 | 117.819 | 14.857 |
| 600 | 48.920 | 125.584 | 20.602 |
| 700 | 51.214 | 132.714 | 25.659 |
| 800 | 54.435 | 140.769 | 30.643 |
| 900 | 56.932 | 148.798 | 36.903 |
| 1000 | 59.481 | 156.020 | 42.783 |

Table 4. Atomic properties 235TCBP

| Atom | B3LYP | HF |
|---|---|---|
| C1 | -0.183575 | -0.207854 |
| C2 | 0.367962 | 0.427156 |
| C3 | 0.219998 | 0.147613 |
| C4 | -0.097587 | -0.029566 |
| C5 | 0.318240 | 0.289660 |
| C6 | 0.498975 | 0.553834 |
| H7 | 0.053297 | 0.057255 |
| H8 | 0.085156 | 0.086567 |
| Cl9 | -0.284528 | -0.292450 |
| Cl10 | -0.273304 | -0.276549 |
| Cl11 | -0.297381 | -0.301765 |
| O12 | -0.708442 | -0.792683 |
| H13 | 0.301188 | 0.338783 |

Table 5. Calculated absorption wavelength λ, excitation energies E and oscillator strengths f of 235TCBP molecule using B3LYP/6-311++G(d,p) level.

| Solvents | λ (nm) | E (ev) | f (a.u) | Major contribution |
|---|---|---|---|---|
| DMSO | 263.78 | 4.7006 | 0.785 | HOMO->LUMO (85%) |
| | 241.26 | 5.1388 | 0.010 | HOMO->LUMO+2 (98%) |
| | 226.98 | 5.4623 | 0.000 | HOMO->LUMO+1 (57%) |
| | 217.28 | 5.7059 | 0.017 | HOMO->LUMO+3 (95%) |
| | 213.82 | 5.7984 | 0.003 | HOMO-1->LUMO+2 (97%) |
| | 207.87 | 5.9643 | 0.790 | HOMO->LUMO+4 (92%) |
| | 198.36 | 6.2503 | 0.010 | HOMO->LUMO+5 (87%) |
| Acetone | 263.79 | 4.6999 | 0.085 | HOMO->LUMO (87%) |
| | 241.26 | 5.1389 | 0.001 | HOMO->LUMO+2 (98%) |
| | 226.90 | 5.4640 | 0.068 | HOMO->LUMO+1 (56%) |
| | 217.64 | 5.6967 | 0.001 | HOMO->LUMO+3 (97%) |
| | 213.76 | 5.8001 | 0.001 | HOMO-1->LUMO+2 (98%) |
| | 207.80 | 5.9664 | 0.003 | HOMO->LUMO+4 (92%) |
| | 198.63 | 6.2418 | 0.001 | HOMO->LUMO+5 (86%) |
| Chloroform | 264.87 | 4.6808 | 0.093 | HOMO->LUMO (85%) |
| | 241.37 | 5.1365 | 0.001 | HOMO->LUMO+2 (98%) |
| | 227.50 | 5.4496 | 0.072 | HOMO->LUMO+1 (56%) |
| | 220.14 | 5.6319 | 0.001 | HOMO->LUMO+3 (96%) |
| | 213.51 | 5.8067 | 0.001 | HOMO-1->LUMO+2 (97%) |
| | 207.53 | 5.9740 | 0.038 | HOMO->LUMO+4 (90%) |
| | 199.98 | 6.1997 | 0.001 | HOMO->LUMO+5 (84%) |

Table 6: Experimental (FT-IR and FT-Raman) wavenumbers and detailed assignments of theoretical wavenumbers of along with potential energy distribution of 235TCBP

| Sy | Infrared region | Raman region | $I^{IR}$ | $S^a$ | B3LYP | Scaled | HF | Scaled | Vibrational assignment |
|---|---|---|---|---|---|---|---|---|---|
| A′ | 3525 vw | | 90.00 | 109.03 | 3831 | 3670 | 4182 | 3792 | γOH(100) |
| A′ | 3080 m | | 1.22 | 68.87 | 3213 | 3078 | 3378 | 3063 | γCH (98) |
| A′ | | 3050 w | 2.26 | 88.87 | 3179 | 3046 | 3344 | 3032 | γCH (99) |
| A′ | 1595 vw | 1595 vw | 30.40 | 31.65 | 1621 | 1594 | 1777 | 1611 | γCC( 71) |
| A′ | 1570 vs | 1570 vw | 0.24 | 24.51 | 1605 | 1578 | 1757 | 1593 | γCC(68) |
| A′ | 1475 vs | | 188.48 | 1.42 | 1504 | 1479 | 1648 | 1494 | γCC(75) |
| A′ | 1375 vs | | 141.01 | 2.48 | 1395 | 1371 | 1514 | 1373 | γCC(65) |
| A′ | 1300 vs | | 2.49 | 1.66 | 1325 | 1302 | 1408 | 1277 | γCC(72) |
| A′ | | 1275 vw | 18.12 | 15.39 | 1293 | 1271 | 1381 | 1252 | γCC(63) |
| A′ | | 1240 vw | 37.77 | 1.72 | 1266 | 1245 | 1317 | 1194 | γCO(75) |
| A′ | 1165 vs | | 124.59 | 9.47 | 1181 | 1161 | 1251 | 1134 | βOH(61) |
| A′ | 1120 vs | | 99.94 | 9.80 | 1143 | 1124 | 1186 | 1076 | βCH(51) |
| A′ | 1070 vs | | 87.56 | 1.99 | 1086 | 1067 | 1169 | 1060 | βCH(57) |
| A′ | | | 10.16 | 5.31 | 935 | 919 | 1022 | 927 | βCCC(46) |
| A′ | 875 vs | | 25.10 | 0.14 | 890 | 875 | 1021 | 926 | βCCC(51) |
| A′ | 820 vw | | 13.61 | 0.26 | 835 | 820 | 956 | 867 | βCCC(52) |
| A′ | 730 vs | | 36.13 | 12.61 | 741 | 728 | 800 | 725 | βCO(48) |
| A″ | | | 0.36 | 0.70 | 697 | 685 | 798 | 723 | φOH(58) |
| A″ | | | 33.87 | 6.80 | 684 | 673 | 741 | 672 | φCH(42) |
| A″ | | 615 s | 0.11 | 0.58 | 628 | 618 | 722 | 654 | φCH(53) |
| A″ | 560 vs | | 15.65 | 1.10 | 569 | 559 | 616 | 558 | φCCC(48) |
| A″ | | 515 vs | 9.71 | 1.04 | 529 | 520 | 573 | 519 | φCCC(36) |
| A″ | 435 m | | 10.31 | 0.09 | 452 | 444 | 503 | 456 | φCCC(39) |
| A″ | | | 2.73 | 13.93 | 394 | 387 | 426 | 386 | φCO(35) |
| A′ | | | 4.34 | 0.15 | 363 | 357 | 412 | 373 | γCCl(61) |
| A′ | | 330 vs | 0.11 | 7.29 | 327 | 321 | 352 | 319 | γCCl(43) |
| A′ | | 302 vw | 100.57 | 1.13 | 304 | 299 | 304 | 276 | γCCl(46) |
| A′ | | | 5.41 | 0.19 | 281 | 276 | 286 | 260 | βCCl(32) |
| A′ | | 230 s | 1.71 | 1.16 | 231 | 227 | 258 | 234 | βCCl(33) |
| A′ | | 202 vs | 0.25 | 0.15 | 208 | 204 | 225 | 204 | βCCl(34) |
| A″ | | 180 vw | 0.02 | 2.78 | 193 | 189 | 208 | 189 | φCCl(37) |
| A″ | | | 0.19 | 0.08 | 144 | 141 | 160 | 145 | φCCl(32) |
| A″ | | | 0.31 | 0.10 | 79 | 78 | 88 | 80 | φCCl(35) |

s: strong; vs: very strong; m: medium; w: weak; vw: very weak. b γ: stretching; β: in-plane bending; φ: out-of-plane bending; $I^{IR}$: Infrared intensity; $S^a$: Raman activity; Sy: Symmetry species

Table .7: Experimental and theoretical probable $^{13}C$ and $^{1}H$ NMR isotropic chemical shifts of compound (atom positions are numbered as in Fig. 1)

| Atom | Experiment | HF/6-311G(d,p) | Atom | Experiment | HF/6-311G(d,p) |
|---|---|---|---|---|---|
| C6 | 158 | 165.5 | H8 | 7.3 | 7.4 |
| C2 | ---- | 152.6 | H7 | 7.1 | 7.2 |
| C4 | ---- | 148.4 | H13 | 5.7 | 5.6 |
| C3 | 138 | 139.3 | | | |
| C5 | ---- | 135.8 | | | |
| C1 | 122 | 123.5 | | | |